Technical Memo

ECMWF
European Centre for Medium-Range Weather Forecasts

891

Summary of the UGROW subproject on tropospheric temperature bias during JJA over the northern hemisphere

L. Magnusson, M. Alonso-Balmaseda, M. Dahoui, R. Forbes, T. Haiden, D. Lavers, I. Sandu, S. Tietsche

March 2022

Series: ECMWF Technical Memoranda

A full list of ECMWF Publications can be found on our web site under:

http://www.ecmwf.int/publications/

Contact: library@ecmwf.int

European Centre for Medium Range Weather Forecasts
Shinfield Park, Reading, Berkshire RG2 9AX, England

Abstract

UGROW is an ECMWF cross-departmental project focused on Understanding systematic error GROWth from hours to seasons ahead. In this sub-topic of the UGROW project we have investigated biases in the lower to mid-tropospheric temperature during the northern hemisphere summers. The bias was investigated across different-time scales and with a range of diagnostic tools. The bias peaks around 700 hPa and grows fastest during the first days of the forecast. The bias mainly appears over land masses in early forecast ranges and has a maximum over eastern Asia. Despite being robust both in terms of day-to-day and year-to-year variability, the investigations so far have not pointed to a clear model error source. The aim of this report is to document the findings about this specific bias during the UGROW project, which will serve as a starting point for future investigations.

1. Introduction

UGROW is an ECMWF cross-departmental project focused on Understanding systematic error GROWth from hours to seasons ahead. It aims to build on and strengthen existing efforts and constitutes an additional channel to bring together scientists from various teams across ECMWF who are interested in identifying ways to enhance predictive skill, in particular at sub-seasonal timescales (weeks 2-4). In 2021, three UGROW sub-topics were selected: Indian Ocean biases, northern hemisphere summer tropospheric temperature biases and the winter Pacific jet stream bias. This report presents results about the bias in the tropospheric temperature appearing over continents in the northern hemisphere during June, July, and August (JJA). Other sub-topics are presented in companion ECMWF Technical Memoranda (Vitart et al.,2022; Mayer et al., in prep).

Biases in atmospheric models can vary with season, geographical location, altitude, and weather flow patterns. Different biases grow at different rates in forecasts and the location can also shift with increasing lead-time. It is therefore important to stratify the verification data and to apply a range of diagnostic tools to understand the signature of the error. The list of tools applied in this report is summarised in Appendix A. This short report documents the characteristics of biases in the lower to mid troposphere (850-500hPa) temperatures that appear during summertime (JJA) over northern hemisphere land masses. This report will mainly be based on forecasts from JJA in 2020. During this season the ECMWF Integrated Forecasting System (IFS) was based on cycle 46r1 until 30 June and 47r1 after. The system consisted of the deterministic (HRES) forecasts with 9km resolution and 137 vertical levels and the ensemble forecasts (ENS), which included one unperturbed member (ENS control) and 50 perturbed members all with 18km resolution and 91 vertical levels. The perturbed members included model perturbations in form of the SPPT scheme (Leutbecher et al., 2017). It is plausible that the difference in resolution and/or the use of SPPT can modulate the biases. In May 2021 the number of vertical levels in ENS was increased to 137 to be the same as in HRES.

The aim of this report is to document the findings about this specific bias during the UGROW project, which will serve as a starting point for future investigations.

2. Results

2.1. Medium-range verification against analysis

Figures 1-3 show different aspects of the biases of HRES during JJA 2020, verified against the ECMWF HRES analysis. The vertical cross-section of the temperature bias on day 2 (Figure 1, left) shows that all latitudes in the northern hemisphere outside the tropics exhibit a warm bias between 700 and 400 hPa. A strong warm bias also appears down to 850 hPa for 30°N-40°N. We will therefore focus our investigation on the 700 hPa level. The warm bias at 700 hPa in 2-day forecasts is most pronounced over most landmasses of the northern hemisphere (Figure 1, right), with the strongest bias found over north-eastern China. At the same time, we see cold biases over large parts of the oceans for this level.

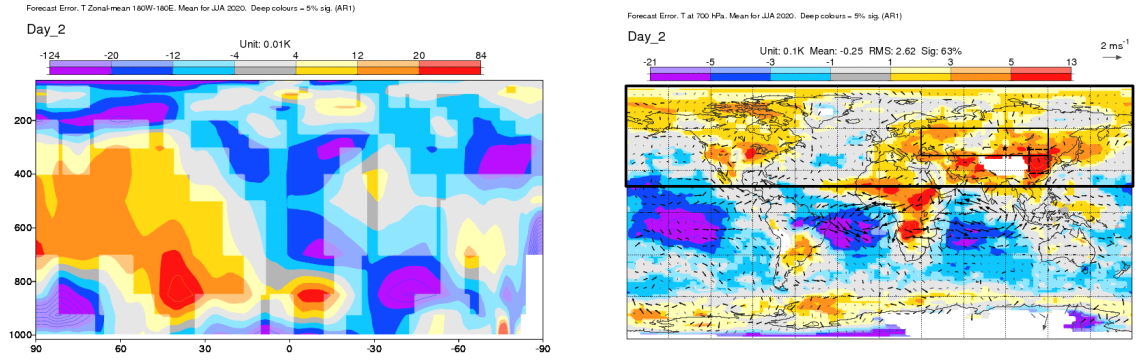

Figure 1. Vertical cross-section (left) and 700-hPa (right) temperature bias for 2-day forecasts for HRES from JJA 2020. Boxes in the right plot indicate regions used in this report. White areas are masked below orography.

Figure 2 (left) shows the lead-time dependence of the bias over the ECMWF verification region for the northern hemisphere extra-tropics (N.Hem, 20°N-90°N, black-thick box in Figure 1 (right). The bias grows fastest over the first four forecast days and seems to further slow down after 10 days in the ENS control (the maximum lead time for HRES is 10 days). Up to day 10 the HRES and ENS control show a similar growth of the error, but with an indication of a larger bias in HRES than ENS control for the longest lead times. At this time (JJA 2020), ENS control had both a lower vertical and horizontal resolution than HRES.

Figure 2 (right) shows the day-4 bias for T700, N.Hem over the past 10 years for HRES with a 30-day running mean applied. A strong seasonality exists in the bias for all the years, with a peak in the summer and close to zero during the boreal winters.

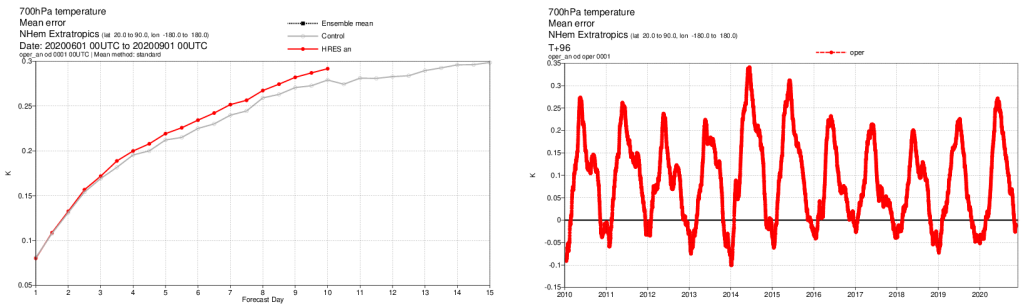

Figure 2. 700-hPa temperature bias for N.Hem in HRES (red) and ENS control (grey) as function of lead-time (left) and time-series for 4-day HRES bias with 30-day running mean applied.

Focusing on the Euro-Asian land masses (40°N-60°N,30°E-120°E, black-thin box in Figure 1 (right)), Figure 3 (top-left) shows the vertical structure of the bias for different levels and lead-times. The diagnostic confirms that the errors are most pronounced around 700 hPa and the growth is fastest over the first four forecast days; the bias is also already present on Day 1.

Figure 3 (top-right) shows forecast departures (observations minus forecasts) from radiosondes in a region over China (28°N-45°N, 105°E-120°E, dashed box in Figure 1 (right)), where the growth of the error (too warm forecasts) follows the same pattern as for the Euro-Asian box but for this region seems to be strongest further down in the troposphere (around 850hPa). The discrepancy in the altitude of the maximum bias for the two diagnostics could be due to different regions, which can give a difference in the ground elevation or differences in physical process(es) responsible for the bias. Further down in this report we will have a closer look at this region over China.

The daily time-series of the 1-day errors against analysis for two locations in central-eastern Asia (45°N,90°E and 45°N,105°E, both marked with stars in Figure 1 (right)) are shown in Figure 3 (bottom). Despite some day-to-day variability in the error, the warm bias is present on most of the days for both locations indicating the systematic nature of the error.

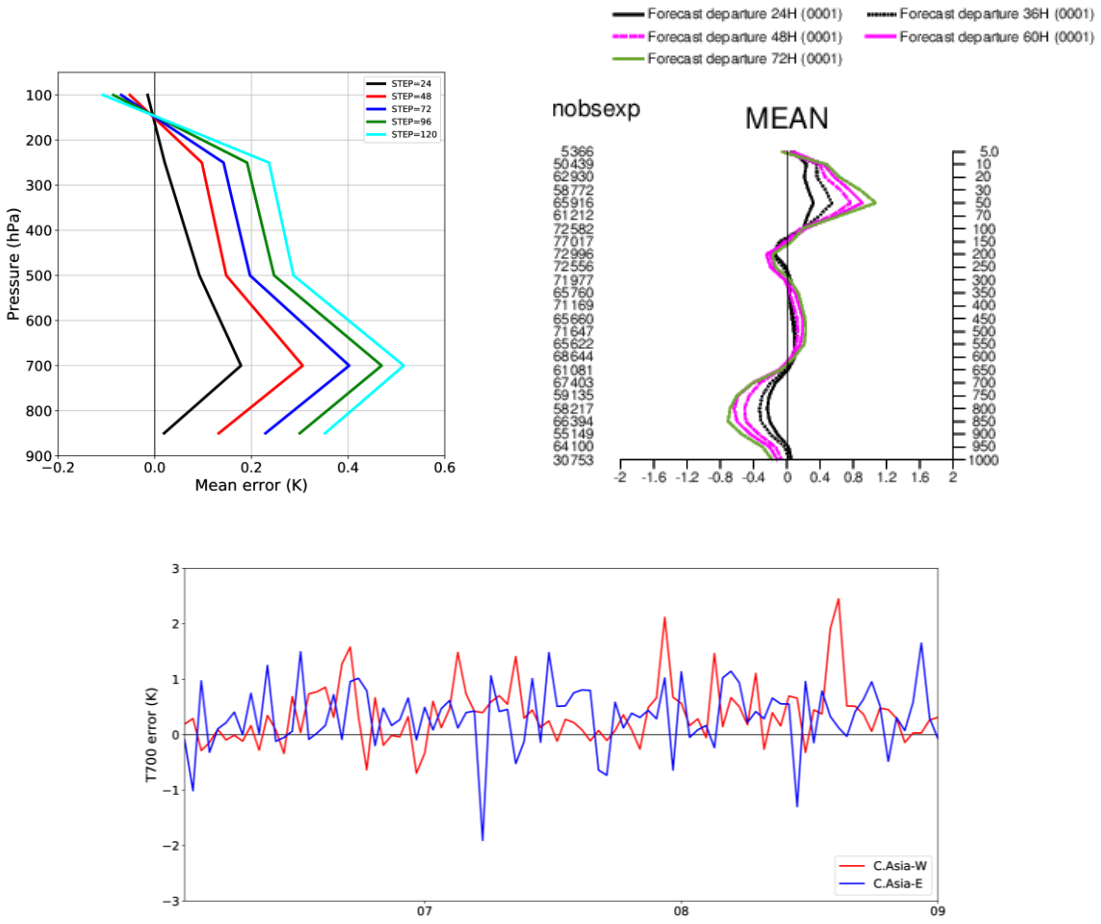

Figure 3. Top-left: Evolution of temperature bias (forecast minus analysis) on different levels and lead-times over central Asia (40°N-60°N,30°N-120°E) in JJA2020. Top-right: Evolution of bias from radiosondes (observations minus forecast) in the region over eastern Asia (28°N-45°N, 105°E-120°E) (top-right). Bottom: T700 error in 1-day forecasts against analysis for two points in central Asia (45°N, 90°E - red and 45°N, 105°E - blue).

2.2. Extended-range verification

Above we found that on a hemispheric scale the bias grows fastest over the first forecast days and starts to saturate after 10 days. In this section we look at a 20-year extended-range reforecast dataset valid for JJA which was produced for 2000-2019 using IFS model cycle 46r1 (June) and 47r1 (July-August). The T700 bias is evaluated for 5-day averages (pentads) against the ERA5 reanalysis. The results are presented for the first three pentads plus the 8th pentad (day 40-44).

On the sub-seasonal scale, the hotspot for the bias over eastern Asia continues to grow and the bias also seems to extend to the east over the Pacific in the 2nd and 3rd pentad (Figure 4). The amplification over the North-western Pacific could potentially be of similar origin as the error during DJF in the jet position over the northern Pacific, which was one of the other UGROW sub-topics and is discussed in

Vitart et al. (2021). We also find relatively large errors over central North America in the extended-range evaluation.

The T700 bias also grows over North America in the lee of the Rockies and over northern Canada. There is also a sign of the bias growing downstream over the Atlantic. In the third forecast pentad (Day 10-14) we also find a strong positive bias of 500-hPa geopotential height over the North Atlantic (Figure 5). One could speculate that this structure could be related to the temperature bias earlier in the forecasts. This bias is also manifested in biases in regime attributions for the Euro-Atlantic sector during JJA, discussed in Büeler et al. (2021). Beyond forecast day 10, they found in ECMWF ensemble forecasts an underestimation in the frequency of the Scandinavian Blocking regime while an overestimation of the regimes involving a ridge over the Atlantic (Atlantic Ridge, Scandinavian Trough and European Blocking).

We have also evaluated the temperature bias in seasonal reforecasts initialised in May 1981-2015 and valid for JJA (Figure 6). On this time scale, the warm bias over China, the North Pacific and North America remains, while a cold bias develops further to the north (around 60°N) over Europe and Asia.

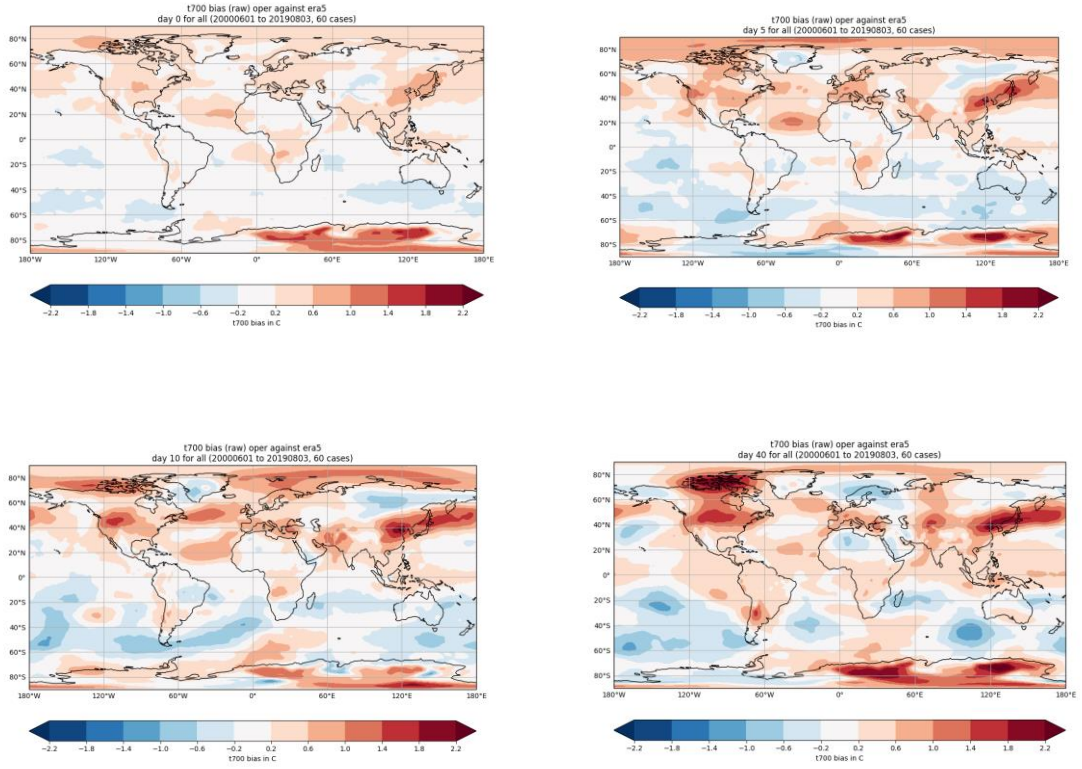

Figure 4. 700-hPa temperature bias in ECMWF reforecasts valid in JJA for day 0-4 (top-left), day 5-9 (top-right), day 10-14 (bottom-left) and day 40-44 (bottom-right).

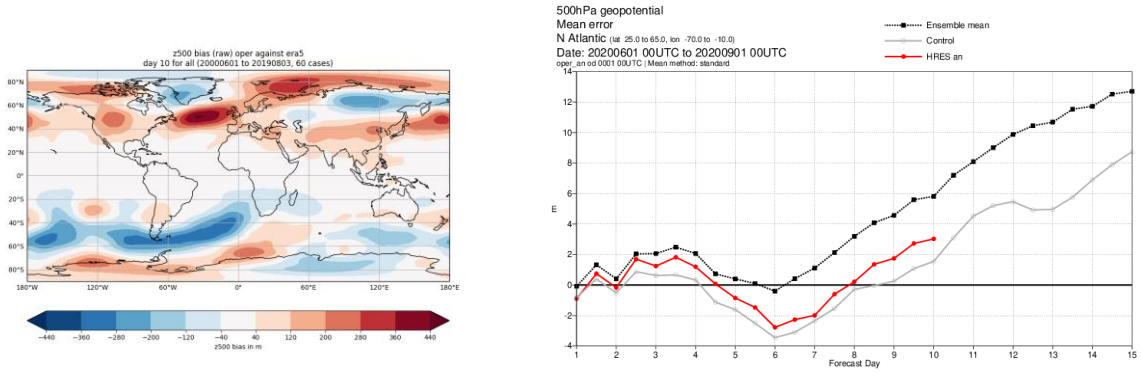

Figure 5. 500-hPa geopotential bias in ECMWF reforecasts valid in JJA for day 10-14 (left) and 500 hPa geopotential height bias for North Atlantic (right) in JJA2020 for HRES (red), ENS CF (grey) and ENS PF mean (black).

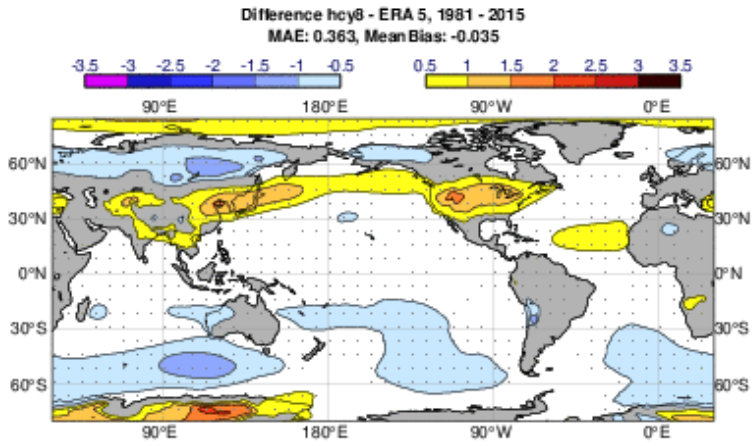

Figure 6. 700-hPa temperature bias in ECMWF seasonal 47r1 reforecasts with resolution TCo199 initialised 1 May 1981-2015 valid in JJA.

2.3. Temperature error over China and possible links to physical processes

In this part we will focus on China where we found the strongest warm bias. Here we will make use of the dataset created in 2018 for the Year of Polar Prediction (YOPP), which is based on the ENS control but includes model tendency output (Bauer et al., 2020). Model tendency output gives information about the individual contributions from different parts of the model (parameterisation schemes and advection). The sum of the tendencies (approximately) gives the forecast evolution and can be compared to the evolution of the atmosphere between analysis times to identify errors.

The bias for 1-day forecasts from the YOPP dataset in JJA2018 averaged in a layer from 850 hPa to 500 hPa is shown in Figure 7. The result confirms a similar pattern as seen for the 700-hPa bias in JJA 2020 in Figure 1 (right).

The forecast error and model tendencies have been explored in the box centred over China (28°N-45°N, 105°E-120°E) and averaged over the layer 850-500 hPa (Figure 8). The region is the same as the one for which the forecast error against radiosondes is shown in Figure 3. For this region and levels, the bias is present for most times of the year during the evaluated 1.5-year YOPP period but is strongest during the spring and first part of the summer. For this part of the year the convection is the dominating model process with a positive tendency on average due to a release of latent heat during condensation. The warming tendency is compensated by the dynamics (horizontal and vertical advection), radiative cooling by the clouds and evaporation of rain by the cloud scheme. Looking at the phasing between the error and the different tendencies, one can first note that the error is lower during the peak of the boreal summer when the convection is strongest. On other hand the error seems to occur during the period when the negative tendency from the cloud scheme (due to evaporation) is largest. It is also the period when we see a negative contribution from the dynamics, either by cold air advection or by local updrafts. Finally, the error occurs during a period with relatively weak radiative cooling from the clouds. It is therefore difficult to draw a conclusion about the process leading to the forecast bias.

Furthermore, a weak negative correlation between temperature errors and humidity errors was found locally over central Asia, but no correlation between the temperature error and the humidity state itself (not shown).

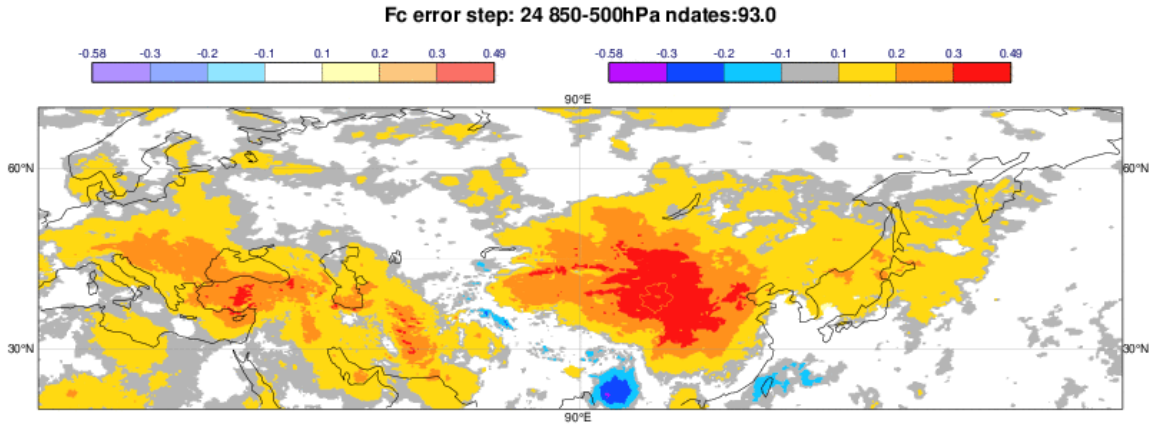

Figure 7. Temperature bias at day 1 averaged between 850-500hPa for YOPP forecast (ENS CF) for JJA2018.

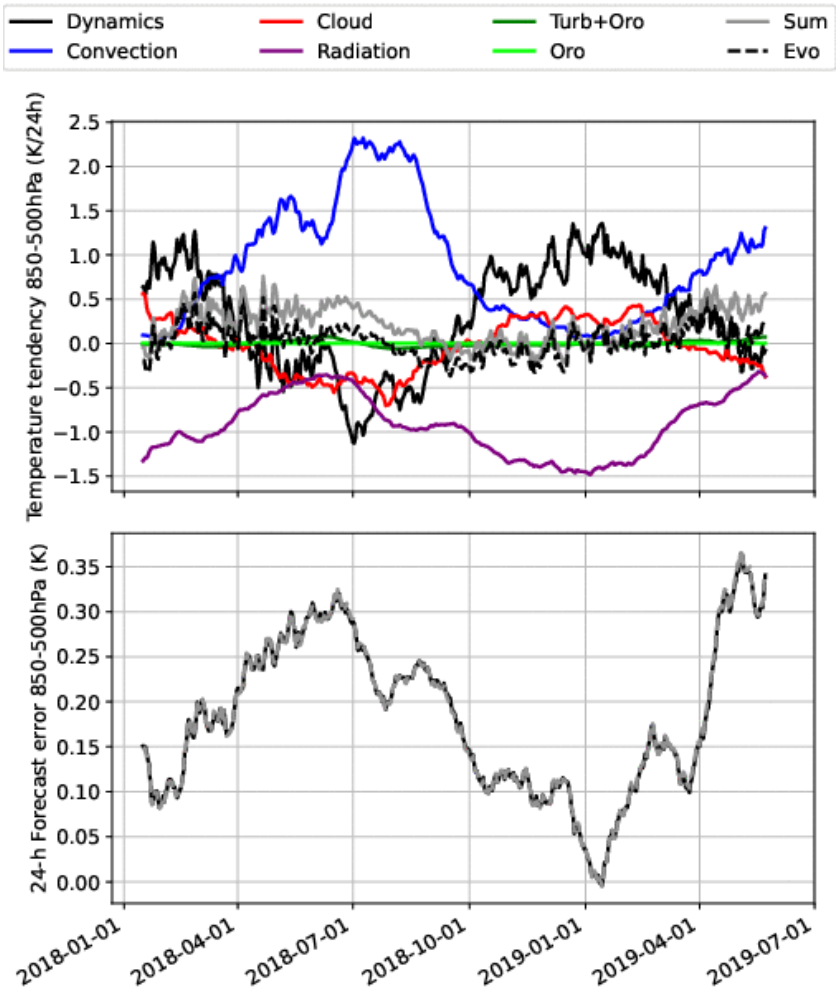

Figure 8. Time series of model tendencies for temperature averaged over the first 24 forecast hours (top) and 24-hour temperature forecast errors (bottom), averaged between 850 hPa and 500 hPa. The top panel also includes the evolution of the temperature over 24 hours. The bottom panel shows the forecast error calculated from the 24-hour forecast output (black) and from the sum of the tendencies minus the evolution (grey dashed). A 30-day running mean is applied to the time-series. All data are averaged inside a box between 28°N-45°N latitude and 105°E-120°E longitude.

Lavers et al. (2021) highlighted southern Asia as a hotspot for a positive precipitation bias (a model wet bias) in the summer, and a figure from the paper is reproduced in Figure 9. The region of the largest wet bias is just south of the hotspot for the temperature errors, suggesting a possible link between the temperature and precipitation, either directly with physical processes or indirectly via the atmospheric flow. One possible synoptic link could be via the Meiyu-Baiu front crossing China in the summer, but no clear day-to-day correlation between the precipitation errors in the Meiyu-Baiu front and the temperature error has been found so far.

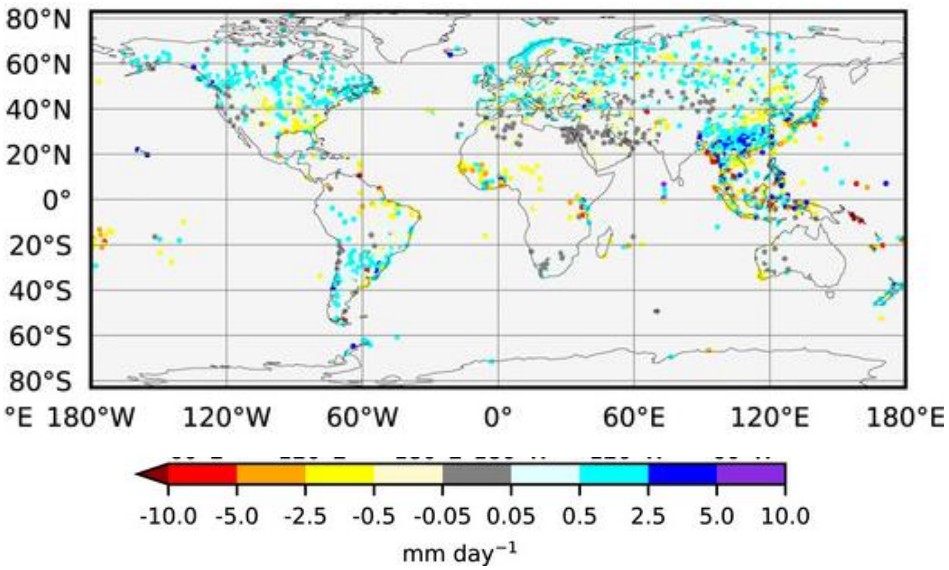

Figure 9. Day 3 precipitation bias in April-September in HRES forecasts.

2.4. Comparison with other centres

The temperature bias has also been explored in forecasts from other modelling centres, using data from the model intercomparison project DIMOSIC (Magnusson et al., 2022, submitted to BAMS). The dataset consists of forecasts from different models initialised from the same (ECMWF) analyses. Figure 10 shows the 700-hPa temperature bias in 3-day forecasts from IFS-47r1, IFS-47r3, DWD-ICON and the MetOffice Unified Model (UM) for start dates in JJA 2018, verified against a multi-analysis based on the TIGGE archive (see Magnusson et al., 2022 for details). The UM shows a similar regional pattern in the warm bias over northern hemisphere continents but with a lower amplitude. The lower amplitude could however be an effect of the model generally being colder than IFS. ICON does not show such a pattern but seems to be too warm over arid regions. Comparing IFS-47r1 and 47r3, we find that the bias is increased in 47r3, which relates to changes in the moist physics in the 47r3 model cycle (Bechtold et al., 2020).

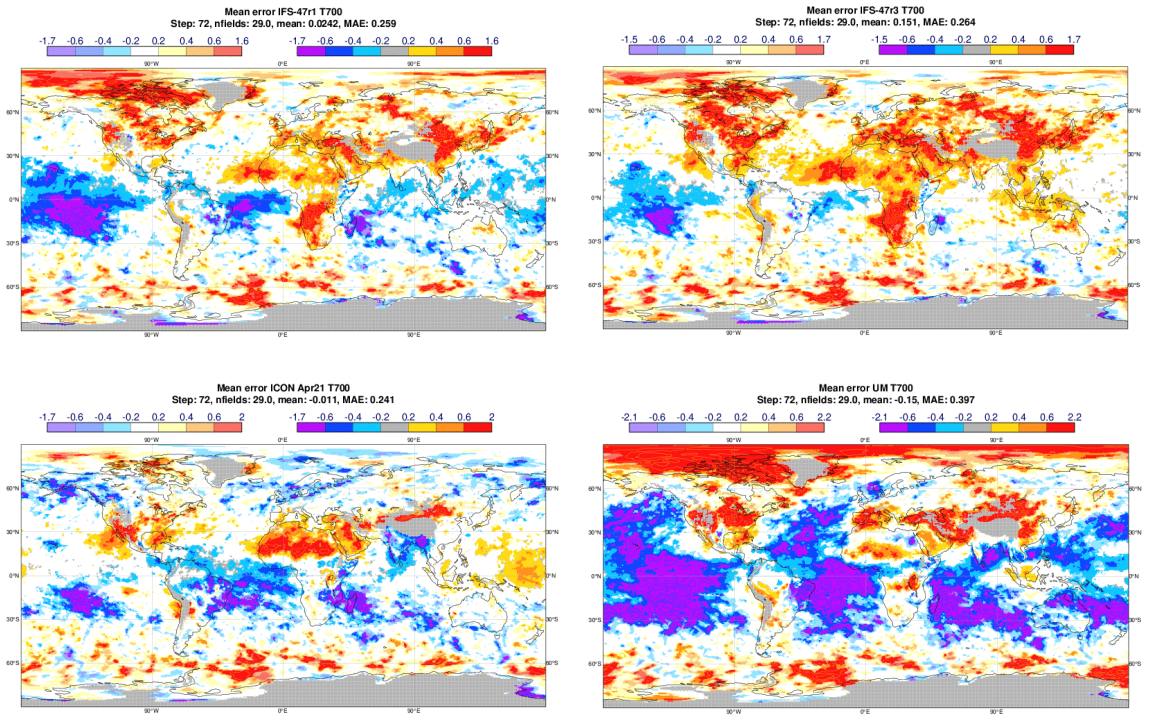

Figure 10. 700 hPa temperature bias for 3-day forecasts from the DIMOSIC dataset (29 start dates in JJA2018) for IFS-47r1 (top-left), IFS-47r3 (top-right), DWD-ICON (bottom-left) and UKMO-UM (bottom-right). Areas below orography are masked in grey.

3. Discussions and future directions

In this sub-topic of the UGROW project we have investigated biases in the lower to mid-tropospheric temperature during the northern hemisphere summers. The bias peaks around 700 hPa and grows fastest during the first days of the forecast. The bias mainly appears over land masses in early forecast ranges and has a maximum over eastern Asia. Despite being robust both in terms of day-to-day and year-to-year variability, the investigations so far have not pointed to a clear error source. It is plausible that the error is a result of several different errors adding up to the structure we see.

However, several future directions were discussed during the UGROW meetings:

- The model tendency budget did not give a clear candidate for the error, as it seems to be an interplay between convection, radiative cooling by clouds and evaporation during the period of the year with the strongest bias. We also discussed the positive precipitation bias in Eastern Asia but noted that the worst region is to the south of the area with the strongest temperature bias. Also, subsequent experiments with improvements to the water conservation in the IFS reduce the precipitation bias over Eastern Asia and cool the upper troposphere but lead to a further small warming in the lower troposphere over land.
- The effect on the flow over and in the lee of orography is another candidate for further explorations, as the strongest biases appear in the lee of the Tibetan plateau and the Rocky Mountains. The orography could also explain that the error appears on different vertical levels for different regions, if the height over ground is an important factor.

- We also found that the warm temperature bias is stronger over land than over ocean. This land-sea contrast in the bias in the short lead-times is striking and should be further explored.
- The impact of different aerosol effects could be considered as the region in China is one of the areas with highest aerosol loads in the northern extra-tropics. However, the bias was also evaluated in CAMS forecasts with prognostic aerosols, but no clear improvement for this region was found (not shown). However this result does not rule out that the error is related to aerosol effects that are not currently included in CAMS forecasts. Initial exploratory experiments have been performed with an alternative cloud condensation nuclei concentration based on the CAMS aerosol climatology, rather than the simpler land/sea contrast with added wind-dependence that is in the operational IFS. This leads to a more realistic geographical distribution of cloud liquid droplet effective radius for the radiation calculations, with smaller cloud droplets over polluted regions, leading to increased shortwave reflection and a cooling of the lower troposphere over east Asia, the USA and Europe. Although this is unlikely to explain all of the warm bias, there is clearly some sensitivity to the cloud effective radius which could be explored further.
- To make further progress, a regime-dependent approach to the evaluation could help to link the growth of the warm bias in different regions more closely to particular physical/dynamical processes; for example, to determine how much of the temperature bias growth in the first day is due to specific cloud regimes (stratocumulus, shallow or deep convection), clear sky absorption or other processes. Additional observation datasets such as top-of-atmosphere shortwave radiation from CERES or radar/lidar from CloudSat-CALIPSO could be used to help to identify errors related to cloud.

The warm summertime bias over continental regions is also present in many other global models both for NWP and climate, as described in the CAUSES project (Ma et al., 2018; Morcrette et al., 2018; Van Weverberg et al., 2018; Zhang et al., 2018). The focus of the CAUSES project was the near-surface and lower-tropospheric warm bias over the central USA in a variety of global models with a regime-dependent evaluation. They concluded the warm bias was related to an overestimation of absorbed solar radiation at the surface, due to a combination of insufficient cloud reflection, clear-sky absorption and underestimation of surface albedo, and also soil moisture evaporation. Although the relative magnitude of the sources of error differed between models, there was a significant role of cloud, either in errors in cloud cover or cloud properties in different regimes. Cloud-related errors were the largest contribution for the IFS over the USA in this study but there is still likely to be a combination of reasons for the IFS warm summer-time bias across the different continents.

In the ECMWF cycle 47r3 the bias at 700 hPa for JJA over N.Hem is almost doubled (0.52K compared to 0.29K for 47r2 for day 10 in JJA 2021), as seen in Figure 11. This increase in bias could partly be due to reduction of compensating errors, as 47r3 reduces the cold bias over sub-tropical oceans. One possibility is that the increased temperature in 47r3 could be related to increased moisture in the atmosphere, but further investigations are needed. One can also note here that the bias is less in the ENS control forecast than HRES that could point to a sensitivity to horizontal model resolution.

To conclude, the lower-to mid troposphere temperature bias over the northern hemispheric summers has been persistent over many years but has further increased in the recent model cycle and might also be worse with higher model resolution. Therefore, we should further investigate the roots of the bias.

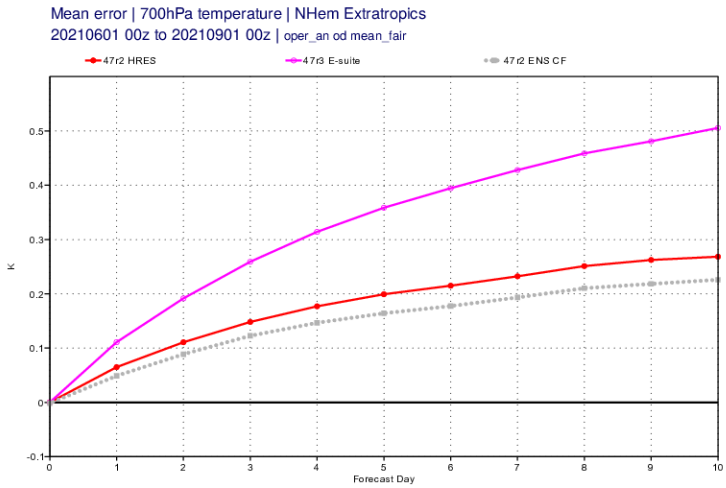

Figure 11. 700-hPa temperature bias for N.Hem in 47r2 HRES (red), 47r3 HRES (purple) and 47r2 ENS control (grey) as function of lead-time.

References

Bauer, P., Sandu, I., Magnusson, L. et al. ECMWF global coupled atmosphere, ocean and sea-ice dataset for the Year of Polar Prediction 2017–2020. Sci Data 7, 427 (2020). https://doi.org/10.1038/s41597-020-00765-y

Bechtold, P., Forbes, R., Sandu, I., Lang, STK., Ahlgrimm, M. (2020). A major moist physics upgrade for the IFS. ECMWF Newsletter 164. https://www.ecmwf.int/en/newsletter/164/meteorology/major-moist-physics-upgrade-ifs

Büeler, D., Ferranti, L., Magnusson, L., Quinting, J. F., & Grams, C. M. (2021). Year-round sub-seasonal forecast skill for Atlantic–European weather regimes. Quarterly Journal of the Royal Meteorological Society, 147(741), 4283–4309. https://doi.org/10.1002/qj.4178

Lavers, D. A., Harrigan, S. and Prudhomme, C. 2021: Precipitation Biases in the ECMWF Integrated Forecasting System. Journal of Hydrometeorology, https://doi.org/10.1175/JHM-D-20-0308.1

Leutbecher, M., Lock, S., Ollinaho, P., Lang, S. T. K., Balsamo, G., Bechtold, P., Bonavita, M., Christensen, H. M., Diamantakis, M., Dutra, E., English, S., Fisher, M., Forbes, R. M., Goddard, J., Haiden, T., Hogan, R. J., Juricke, S., Lawrence, H., MacLeod, D., … Weisheimer, A. (2017). Stochastic representations of model uncertainties at ECMWF: State of the art and future vision. Quarterly Journal of the Royal Meteorological Society, 143(707), 2315–2339. https://doi.org/10.1002/qj.3094

Ma, H.-Y., Klein, S. A., Xie, S., Zhang, C., Tang, S., Tang, Q., et al (2018). CAUSES: On the role of surface energy budget errors to the warm surface air temperature error over the Central U.S. *J. Geophys. Res.: Atmospheres*, 123. https://doi.org/10.1002/2017JD027194

Morcrette, C. J., Van Weverberg, K., Ma, H.-Y., Ahlgrimm, M., Bazile, E., Berg, L. K., et al. (2018). Introduction to CAUSES: Description of weather and climate models and their near-surface temperature errors in 5 day hindcasts near the Southern Great Plains. *J. Geophys. Res.: Atmospheres*, 123. https://doi.org/10.1002/2017JD027199

Van Weverberg, K., Morcrette, C. J., Petch, J., Klein, S. A., Ma, H.-Y., Zhang, C., et al. (2018). CAUSES: Attribution of surface radiation biases in NWP and climate models near the U.S. Southern Great Plains. *J. Geophys. Res.: Atmospheres*, 123. https://doi.org/10.1002/2017JD027188

Vitart F., Emerton, R., Rodwell, M., Alonso-Balmaseda, M., Haiden, T., Johnson, S., Magnusson, L., Roberts, C. D., Sandu, I. (2022). Investigating biases in the representation of the Pacific sub-tropical jet stream and associated teleconnections (a UGROW sub-project), ECMWF Technical Memorandum 889

Zhang, C., Xie, S., Klein, S. A., Ma, H.-y., Tang, S., Van Weverberg, K., et al. (2018). CAUSES: Diagnosis of the summertime warm bias in CMIP5 climate models at the ARM Southern Great Plains site. *J. Geophys. Res.: Atmospheres*, 123, 2968– 2992. https://doi.org/10.1002/2017JD027200

Appendix A - ECMWF Diagnostic tools used in for this report

- Diagnostic Explorer (maps of operational errors)
- Quaver (aggregated operational errors)
- Obstat (short-range forecast errors against radiosondes)
- STVL database (precipitation errors)
- CEPDIAG (extended-range errors)
- Multiyear suite (seasonal forecast errors)
- Tailored tools for DIMOSIC and YOPP tendency diagnostics
- Tailored tools for medium-range verification (bias profiles, correlations)